Journal of the Iranian Chemical Society
https://doi.org/10.1007/s13738-020-01878-2

ORIGINAL PAPER

The immobilized Ni(II) species on thiourea functionalized copper ferrite: a reusable nanocatalyst for synthesis of biscoumarins under solvent-free conditions

Behzad Zeynizadeh[1] · Morteza Hasanpour Galehban[1] · Zahra Shokri[1]

Received: 2 February 2019 / Accepted: 12 February 2020

Abstract
In this study, nanoparticles of $CuFe_2O_4$@SiO_2@PTMS@Tu@Ni(II) as the reusable magnetic catalyst were prepared. Synthesis of the Ni(II)–$CuFe_2O_4$ system was carried out through a five-step procedure including the preparation of $CuFe_2O_4$ as the prime magnetic core, layering of silica, 3-chloropropyltrimethoxysilane and thiourea and finally the immobilization of $Ni(OAc)_2{\cdot}4H_2O$. The prepared nanocomposite system was then characterized using FT-IR, SEM, EDX, XRD, VSM, ICP-OES and TGA/DSC analyses. Catalytic activity of $CuFe_2O_4$@SiO_2@PTMS@Tu@Ni(II) was further studied toward synthesis of biscoumarin materials by a domino Knoevenagel–Michael reaction of 4-hydroxycoumarin with aromatic and heterocyclic aldehydes under solvent-free conditions (70 °C) within 15–30 min. The applied nanocomposite system was easily and magnetically separated from the reaction mixture and reused for six consecutive cycles without the significant loss of its catalytic activity.

Keywords Biscoumarins · $CuFe_2O_4$ · Knoevenagel–Michael · Ni(II) · Thiourea

Introduction

Transition metal elements and their complexes due to prominent biological properties such as antifungal and antibacterial activities as well as the applicability in sensors, optoelectronics, magnetic devices and drug delivery systems have attracted the considerable interest of numerous scientists [1–7]. Consequently, nanomaterials containing transition metals due to inherent electronic configuration and high surface energy of the existing metals and the huge surface area to volume ratio have the eligibility to consider as the more efficient catalyst systems to promote chemical reactions [8]. Despite this, they have a strong tendency for agglomeration to produce bulk counterparts. In this situation, the surface area of nanoparticles (NPs) and catalytic activity of the applied catalyst systems are intensively decreased [9]. Overcoming of these drawbacks needs, the immobilization of transition metals NPs on solid supports to prevent aggregation of nanoparticles and preserve their original characteristics. In this area, the application of carbon materials [10–12], polymers [13–16], zeolites [17–19], resins [20], metal oxides [21, 22] and clay minerals [23–25] was successfully reported for the titled strategy.

Nowadays, the usefulness of spinel ferrites with a general formula of MFe_2O_4 (M = Fe, Cu, Co, Ni, Zn, Mg and Mn) in pigments, gas sensors, ferrofluids, drug delivery and catalysis has gained the considerable interests in academic and industrial points of view [26–32]. Among the spinel ferrites, $CuFe_2O_4$ is a more desirable transition bimetallic oxide. Because, this magnetic material has the advantages in terms of high thermal stability (up to 900 °C), unique magnetic characteristic and synergic chemical reactivity of copper and iron to catalyze transformation of functional groups [33–38].

Over the past years, coumarins have been considered as the prominent biological active materials [39–44]. Among the coumarins, biscoumarin materials also exhibited the significant pharmacological activities such as antibacterial [45–47], antifungal [47], anti-inflammatory [48], anticoagulant [49], antitumor [50], anti-HIV [51–53], cytotoxic, enzyme [47, 54, 55] and urease [56] inhibition, radical scavenger and chain-breaking anti-oxidants [57]. Synthesis of biscoumarin materials is usually carried out through a

✉ Behzad Zeynizadeh
bzeynizadeh@gmail.com

[1] Faculty of Chemistry, Urmia University, Urmia 5756151818, Iran

Published online: 21 February 2020

domino Knoevenagel–Michael reaction of 4-hydroxycoumarin with aromatic aldehydes in the presence of a promoter system. The literature review shows that using $ZnCl_2$ [58], $Zn(proline)_2$ [59], I_2 [60], *n*-Bu_4NBr [61], P4VPy-CuO NPs [62], sulfated titania [63], phosphotungstic acid [64], silica gel [65], silica sulfuric acid NPs [66], silica-supported Preyssler NPs [67], silica-bonded *N*-propylpiperazine sodium *n*-propionate [68], silica-supported sodium hydrogen sulfate and indion 190 resin [69], *p*-toluenesulfonic acid [70], sulfonated rice husk ash (RHA-SO_3H) [71], sodium dodecyl sulfate (SDS) [72], *n*-dodecylbenzene sulfonic acid (DBSA) [73], propane-1,2,3-triyl-tris (hydrogen sulfate) [74], triethylammonium hydrogen sulfate [75], graphene oxide nanosheets [76], mesoporous acid-activated montmorillonite K10 [77], nano Fe_3O_4@ZrO_2–H_3PO_4 [78], mesoporous FeTUD-1 [79], task-specific ionic liquids [80], benzimidazolium-based SO_3H-functionalized ionic liquids [PSebim][OTf] [81], tetramethylguanidium-based ionic liquids [82], $[MIM(CH_2)_4SO_3H][HSO_4]$ [83] has been successfully utilized to promote the synthesis of biscoumarin materials.

Although most of the reported methods have the own advantages/shortcomings; however, the development of environmentally friendly methods is one of the subjects of green chemistry and therefore motivates new challenges toward synthesis of biscoumarin materials. Therefore, in line with the outlined strategies and continuation of our research programs directed to the immobilization of transition metals species on magnetic materials [37, 38, 77, 84–94], herein, we wish to introduce the synthesis and characterization of magnetically nanoparticles (MNPs) of $CuFe_2O_4$@SiO_2@PTMS@Tu@Ni(II). At the next, catalytic activity of the prepared nanocomposite system was investigated toward one-pot Knoevenagel–Michael reaction of 4-hydroxycoumarin with aromatic and heterocyclic aldehydes under solvent-free conditions (Fig. 1).

Experimental

General

All substrates and solvents were purchased from chemical companies in high quality and they were used without further purification. ^1H, ^{13}C NMR and FT-IR spectra were recorded on 300 MHz Bruker Avance and Thermo Nicolet Nexus 670. Magnetic property of the samples was determined using vibrating-sample magnetometer (VSM, Meghnatis Daghigh Caviar Co., Iran) under magnetic fields up to 20 kOe. Morphology of the particles was examined via the obtained SEM images from FESEM-TESCAN MIRA3 instrument. Chemical composition of the samples was determined by EDX analysis. X-ray diffraction (XRD) analysis was carried out on X'PertPro Panalytical diffractometer in 40 kV and 30 mA with a CuKα radiation ($\lambda = 1.5418$ Å). Elemental analysis of Cu and Ni species was carried out by inductively coupled plasma–optical emission spectrometry (ICP-OES, Optima 7300D). The irradiation of ultrasound was carried out on SOLTEC SONICA 2400MH S3 (305 W).

Synthesis of $CuFe_2O_4$@SiO_2 MNPs

Magnetically nanoparticles of $CuFe_2O_4$ were primarily synthesized via a chemical co-precipitation method using $FeCl_3 \cdot 6H_2O$ and $CuCl_2 \cdot 2H_2O$ [36]. Then, layering of silica was carried out on nanocores of $CuFe_2O_4$. For doing, the obtained $CuFe_2O_4$ MNPs (1.5 g) in deionized water (20 mL) were sonicated for 30 min. Subsequently, isopropanol (200 mL), PEG-400 (5.36 g), distilled water (20 mL), aqueous ammonia (10 mL, 25 wt%) and tetraethyl orthosilicate (TEOS, 2 mL) were, respectively, added to the prepared suspension. The mixture was stirred at room temperature for 28 h. The resulting $CuFe_2O_4$@SiO_2 MNPs were magnetically separated, washed with distilled water and aqueous ethanol 96% and then dried under air atmosphere.

Preparation of $CuFe_2O_4$@SiO_2@PTMS@Tu@Ni(II) MNPs

Magnetically nanoparticles of $CuFe_2O_4$@SiO_2 (1.7 g) were dispersed in absolute EtOH (120 mL). 3-Chloropropyltrimethoxysilane (3.4 mL) was then added and the resulting mixture was irradiated by ultrasound for 60 min. The mixture was continued to stir under reflux and N_2 atmosphere for 20 h. The prepared nanoparticles of $CuFe_2O_4$@SiO_2@PTM-Cl were washed with distilled water and aqueous ethanol 96% and then dried under air atmosphere.

Next, the magnetic nanoparticles of $CuFe_2O_4$@SiO_2@PTM-Cl (1 g) in absolute EtOH (50 mL) were dispersed by sonication for 20 min. K_2CO_3 (2.5 mmol) and thiourea (2.5 mmol) were added and the resulting mixture was

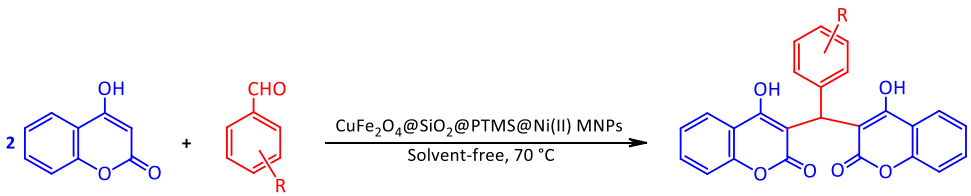

Fig. 1 Synthesis of biscoumarin materials catalyzed by $CuFe_2O_4$@SiO_2@PTMS@Tu@Ni(II) MNPs

stirred under reflux conditions for 20 h (N_2 atmosphere). The obtained $CuFe_2O_4$@SiO_2@PTMS@Tu MNPs were washed with distilled water and aqueous ethanol 96% and then dried under air atmosphere.

Finally, the magnetic nanoparticles of $CuFe_2O_4$@SiO_2@PTMS@Tu (1 g) were sonicated in absolute EtOH (25 mL) and were mixed with an aqueous solution of $Ni(OAc)_2{\cdot}4H_2O$ (0.5 g in a mixture of EtOH:H_2O/2:2 mL). The resulting mixture was stirred under reflux conditions for 20 h. The obtained nanoparticles of $CuFe_2O_4$@SiO_2@PTMS@Tu@Ni(II) were magnetically separated, washed with distilled water and aqueous ethanol 96% and then dried at 50 °C.

A typical procedure for synthesis of biscoumarin materials

In an experimental tube, a mixture of benzaldehyde (1 mmol), 4-hydroxycoumarin (2 mmol) and $CuFe_2O_4$@SiO_2@PTMS@Tu@Ni(II) MNPs (10 mg) was stirred and heated in an oil bath (70 °C). After completion of the reaction within 15 min (monitored by TLC), EtOAc was added and the resulting mixture was stirred for 5 min. The nanocatalyst was magnetically separated from the reaction mixture. Evaporation of the solvent under reduced pressure followed by recrystallization of the crude product from hot EtOH affords the pure biscoumarin 3,3′-(phenylmethylene)-bis(4-hydroxy-2H-chromen-2-one) in 95% yield (Table 2, entry 1).

Results and discussion

Synthesis of $CuFe_2O_4$@SiO_2@PTMS@Tu@Ni(II) MNPs

The study was started by synthesis of $CuFe_2O_4$@SiO_2@PTMS@Tu@Ni(II) MNPs via a five-step procedure (Fig. 2): (i) magnetically nanoparticles of $CuFe_2O_4$ was prepared through a chemical co-precipitation of $FeCl_3{\cdot}6H_2O$ and $CuCl_2{\cdot}2H_2O$ in an aqueous solution

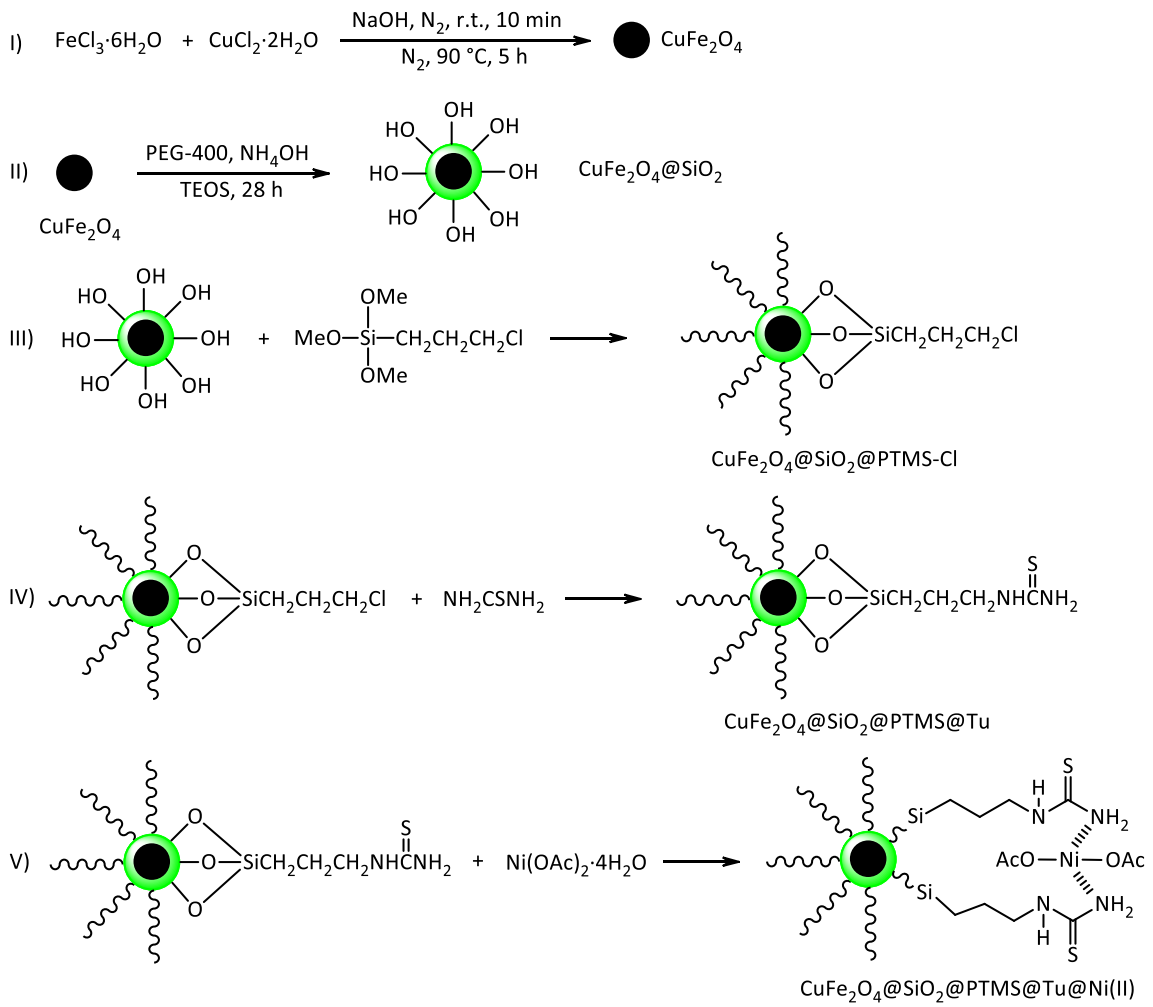

Fig. 2 Synthetic diagram of $CuFe_2O_4$@SiO_2@PTMS@Tu@Ni(II) MNPs

of NaOH, (ii) layering of silica around nanocores of $CuFe_2O_4$ using tetraethyl orthosilicate (TEOS), (iii) surface-linking of $CuFe_2O_4@SiO_2$ with 3-chloropropyltrimethoxysilane (PTMS-Cl), (iv) linking of thiourea with the immobilized 3-chlorotrimethoxysilane on $CuFe_2O_4@SiO_2$ and (v) immobilization of $Ni(OAc)_2{\cdot}4H_2O$ on $CuFe_2O_4@SiO_2@PTMS@Tu$ giving the nanocomposite of $CuFe_2O_4@SiO_2@PTMS@Tu@Ni(II)$. In continuation, characterization of the Ni(II)–$CuFe_2O_4$ system was carried out using FT-IR, SEM, EDX, XRD, VSM, ICP-OES and TGA/DSC analyses.

FT-IR analysis

Fourier transform infrared spectroscopy as a primarily tool was used for functional groups and structural elucidation of $CuFe_2O_4$, $CuFe_2O_4@SiO_2@PTMS@Tu$ and $CuFe_2O_4@SiO_2@PTMS@Tu@Ni(II)$ MNPs. In FT-IR spectrum of $CuFe_2O_4$ MNPs (Fig. 3a), the bands at 460 and 583 cm^{-1} are attributed to bending vibration of Cu–O and Fe–O bonds, respectively. As well, a broadband around 3426 cm^{-1} is devoted to the stretching vibration of the adsorbed water or surface hydroxyl groups [95]. In FT-IR spectrum of $CuFe_2O_4@SiO_2@PTMS@Tu@Ni(II)$ MNPs (Fig. 3b), a broad absorbance at 583 cm^{-1} is devoted to

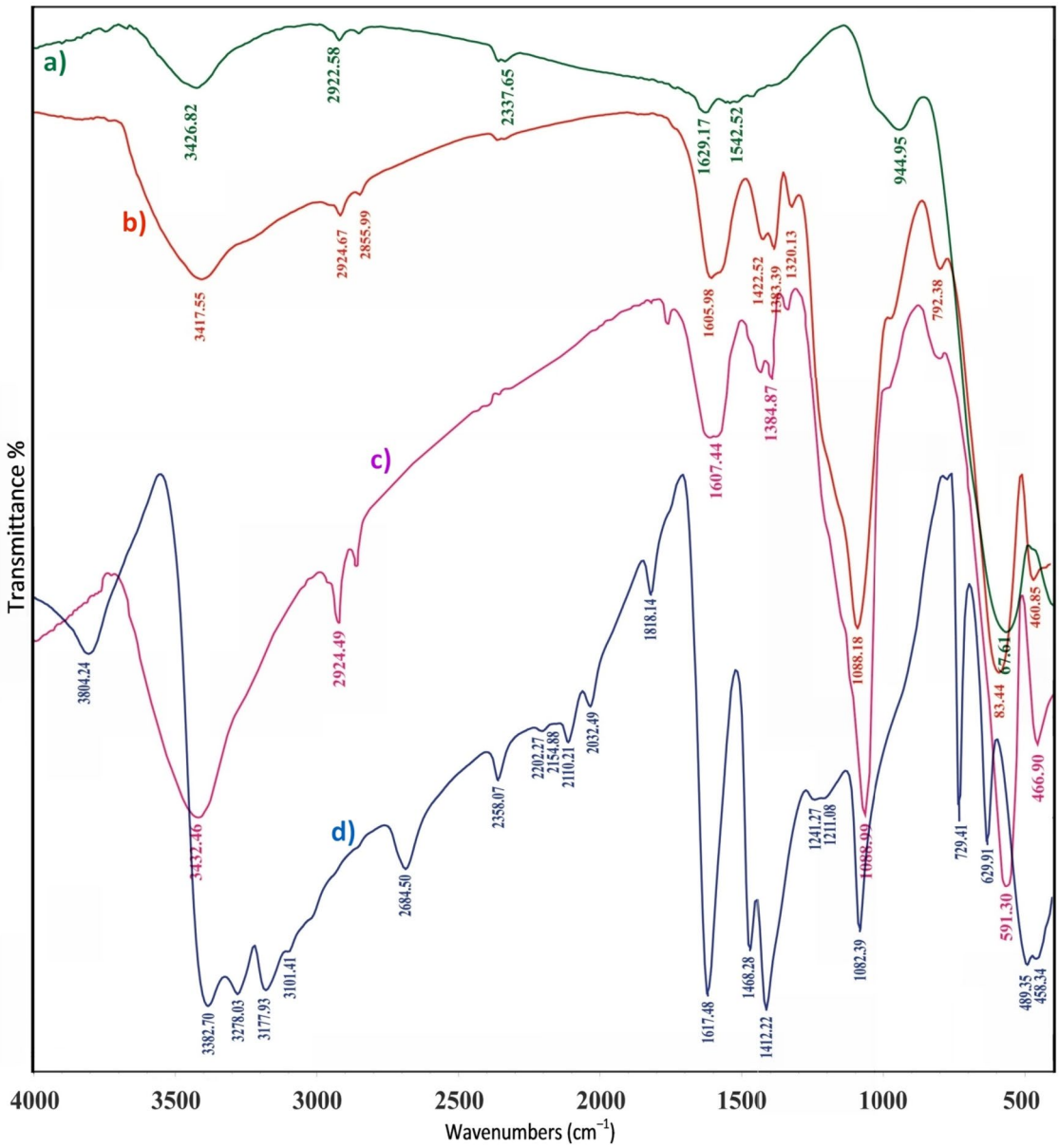

Fig. 3 FT-IR spectra of (a) $CuFe_2O_4$ and (b) $CuFe_2O_4@SiO_2@PTMS@Tu@Ni(II)$, (c) $CuFe_2O_4@SiO_2@PTMS@Tu$ and (d) thiourea

bending vibration of Cu–O, Fe–O and Ni–O. The layering of silica around nanocores of copper ferrite and the linkage of propylsiloxy groups are also verified by a strong absorbance band at 1080 cm^{-1}. Consequently, two bands around 1422 and 1605 cm^{-1} are also defined to symmetric and asymmetric vibrations of C=S in thiourea [96]. Comparing the FT-IR spectrum of $CuFe_2O_4$@SiO_2@PTMS@Tu@Ni(II) (Fig. 3b) with that of $CuFe_2O_4$@SiO_2@PTMS@Tu (Fig. 3c) shows that the peak pattern of both spectra is the same; however, intensity of the peaks around 3432 and 2924 cm^{-1} showing the stretching vibrations of NH_2 and the aliphatic propyl groups, respectively, was increased. Through the immobilization of Ni(II) species, in addition, a little shifting (1–3 cm^{-1}) of the signals to lower frequencies in FT-IR spectrum of $CuFe_2O_4$@SiO_2@PTMS@Tu@Ni(II) is observable. In this context, FT-IR spectrum of thiourea (Fig. 3d) representing the signal position of NH_2, C–N and C=S bonds demonstrates that the immobilization of thiourea on the surface of $CuFe_2O_4$@SiO_2@PTMS MNPs was successfully taken place. Based on this evaluation, therefore, the immobilization of thiourea, propylsiloxy and silica layer on nanocores of $CuFe_2O_4$ was successfully verified.

SEM analysis

Next, the porosity and surface morphology of $CuFe_2O_4$@SiO_2@PTMS@Tu@Ni(II) MNPs was studied using scanning electron microscopy (SEM) technique. Illustrated images in Fig. 4 show that surface of Ni(II)–$CuFe_2O_4$ MNPs has the extreme porosity; however, to some extent, the agglomeration of nanoparticles was led to the formation of bulk segments. The nanoparticles have harsh/irregular shapes and they are distributed in the range of 15–34 nm.

EDX and ICP-OES analysis

In continuation, the elemental profile of $CuFe_2O_4$@SiO_2@PTMS@Tu@Ni(II) MNPs was also determined by energy-dispersive X-ray (EDX) analysis. Depicted graph in Fig. 5 shows that all the required elements (C, N, O, Fe, Si, Cu, S and Ni) are present in composition of the nanocatalyst, and therefore, it demonstrates the successful preparation of $CuFe_2O_4$@SiO_2@PTMS@Tu@Ni(II) MNPs. Consequently, the exact amount of Ni (19.9%) and Cu (9.7%) was determined using inductively coupled plasma–optical emission spectroscopy (ICP-OES).

XRD analysis

At the next, the phase purity and crystallinity character of $CuFe_2O_4$ and $CuFe_2O_4$@SiO_2@PTMS@Tu@Ni(II)

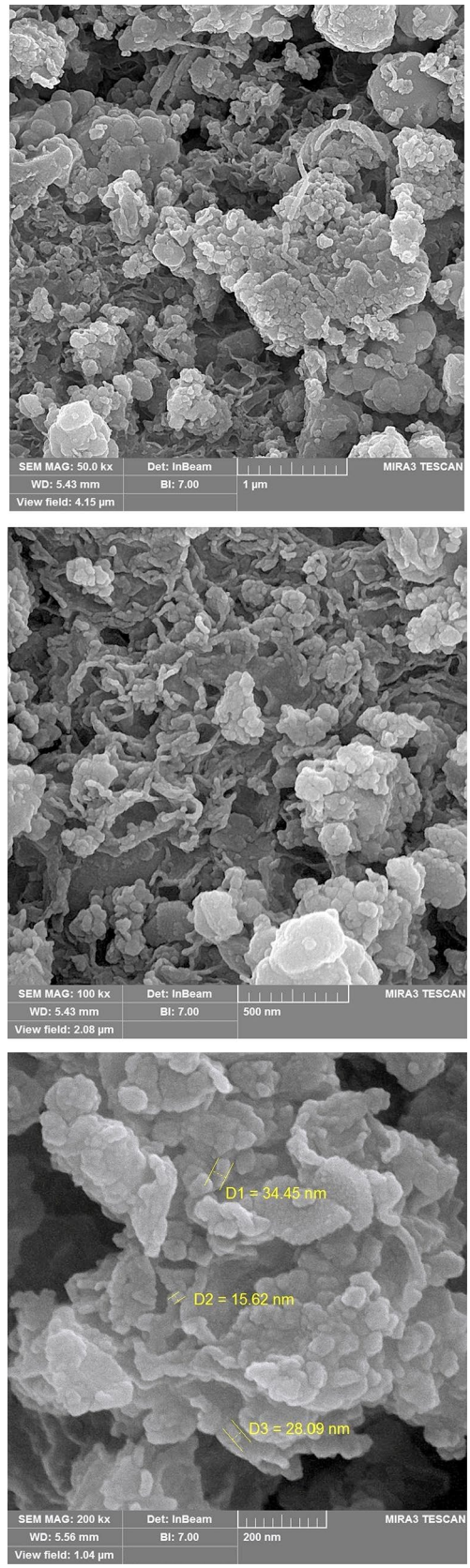

Fig. 4 SEM images of $CuFe_2O_4$@SiO_2@PTMS@Tu@Ni(II) MNPs

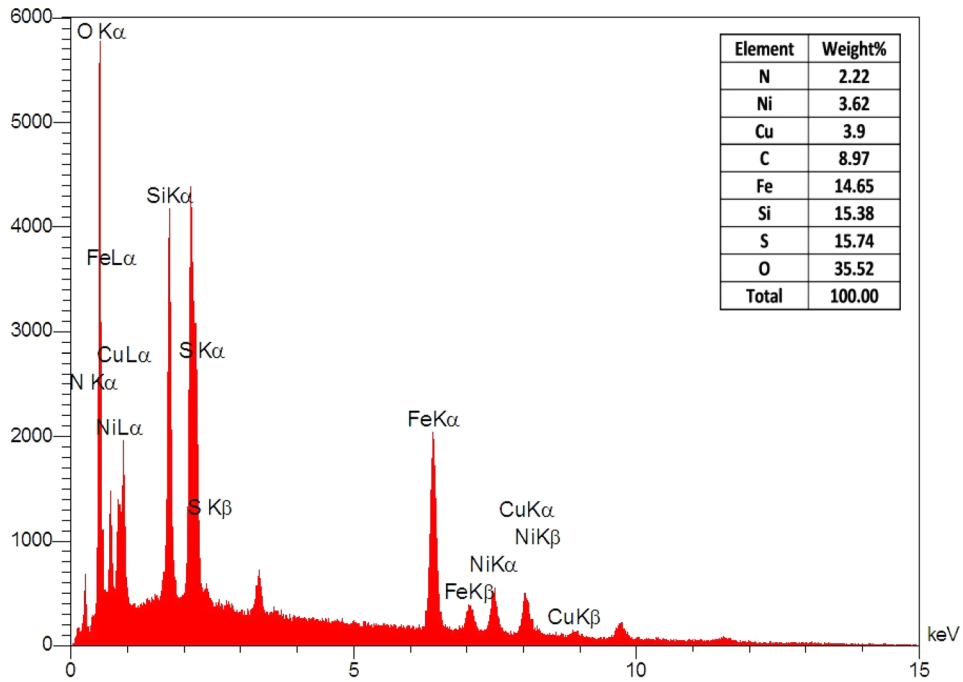

Fig. 5 EDX spectrum of $CuFe_2O_4$@SiO_2@PTMS@Tu@Ni(II) MNPs

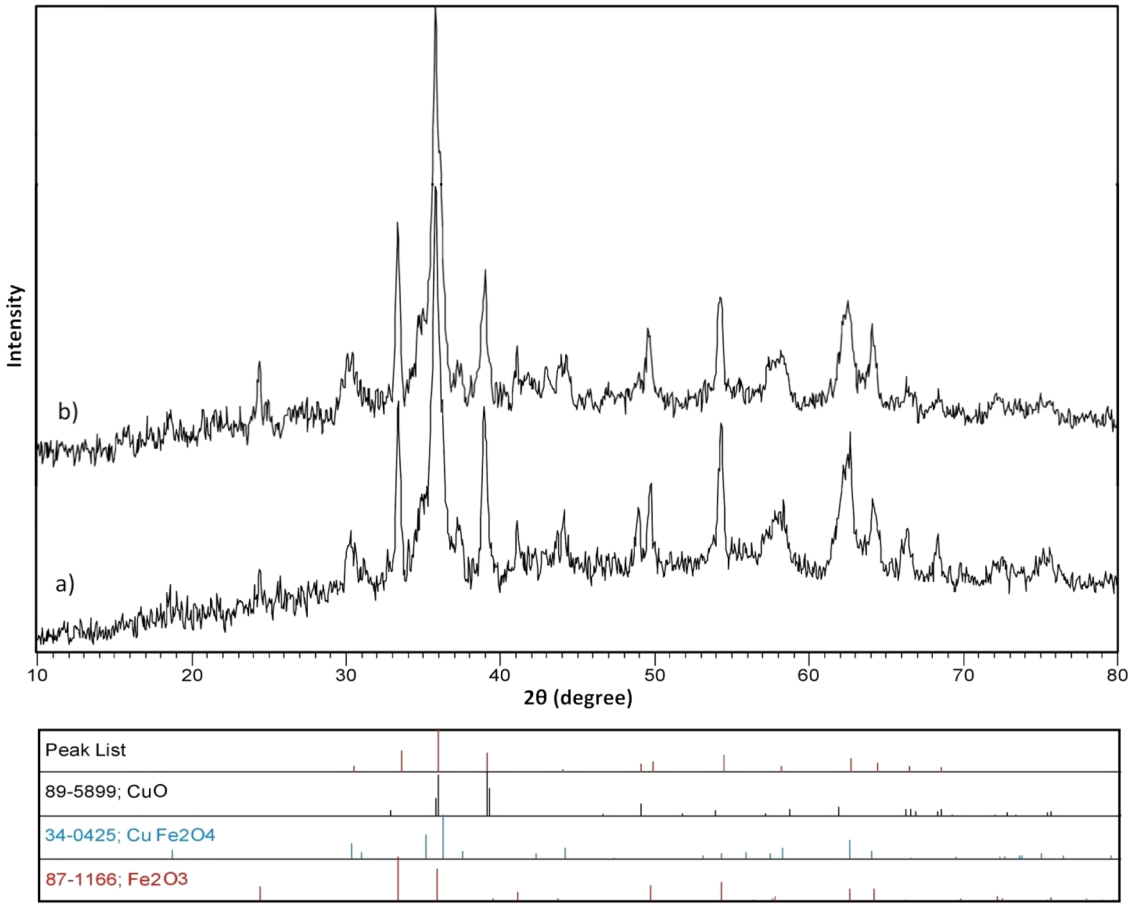

Fig. 6 XRD patterns of (a) $CuFe_2O_4$ and (b) $CuFe_2O_4$@SiO_2@PTMS@Tu@Ni(II) MNPs

MNPs were studied using X-ray diffraction (XRD) analysis (Fig. 6). The XRD pattern of $CuFe_2O_4$ (Fig. 6a) represents the signals at $2\Theta = 19.01°$, 30.2°, 35.8°, 43.3°, 54.3°, 57.9° and 62.6° corresponding to the reflection planes of (1 1 1), (2 2 0), (3 1 1), (4 0 0), (4 2 2), (5 1 1), and (4 4 0), respectively. Comparison of the pattern with the standard one of cubic spinel $CuFe_2O_4$ (JCPDS 77–0010) [97] illustrates the prepared laboratory sample of copper ferrite has the impurity of CuO and Fe_2O_3. Thus, the phase purity of the $CuFe_2O_4$ sample was slightly downed; however, its crystallinity character, based on the signal shapes, is high. Moreover, comparing the XRD pattern of $CuFe_2O_4$@SiO_2@PTMS@Tu@Ni(II) (Fig. 6b) with the laboratory sample of $CuFe_2O_4$ (Fig. 6a) represents that during the layering of SiO_2@PTMS@Tu moiety and anchoring Ni(II) species, the cubic spinel structure of $CuFe_2O_4$ remained intact. The pattern analysis also shows that the crystallinity character and phase purity of the Ni(II)–$CuFe_2O_4$ and $CuFe_2O_4$ are the same. In this context, the average crystallite size of $CuFe_2O_4$@SiO_2@PTMS@Tu@Ni(II) MNPs (based on the Debye–Scherrer equation) was calculated 54.35 nm, while $\lambda = 0.1542$ nm, $2\Theta = 35.783°$, FWHM = 0.2558°, $\beta = 0.00446$ rad).

VSM analysis

Magnetic properties of $CuFe_2O_4$ and $CuFe_2O_4$@SiO_2@PTMS@Tu@Ni(II) MNPs were determined using vibrating-sample magnetometer (VSM) analysis in an applied magnetic field up to 20 KOe. Based on this analysis (Fig. 7), the saturation magnetization (M*s*) values of $CuFe_2O_4$ and $CuFe_2O_4$@SiO_2@PTMS@Tu@Ni(II) MNPs were determined 13.49 and 5.45 emu g^{-1}, respectively. Comparison of the M*s* values clearly shows that during the layering of magnetic nucleuses with nonmagnetic species, the saturation magnetization of the final nanocomposite was notably decreased. Although the value was decreased, it was enough for any magnetic separation. It is also concluded that, because of the existing of hysteresis loop of magnetization, the prepared laboratory samples of $CuFe_2O_4$ and $CuFe_2O_4$@SiO_2@PTMS@Tu@Ni(II) MNPs have the characteristic of soft ferromagnetic materials [98].

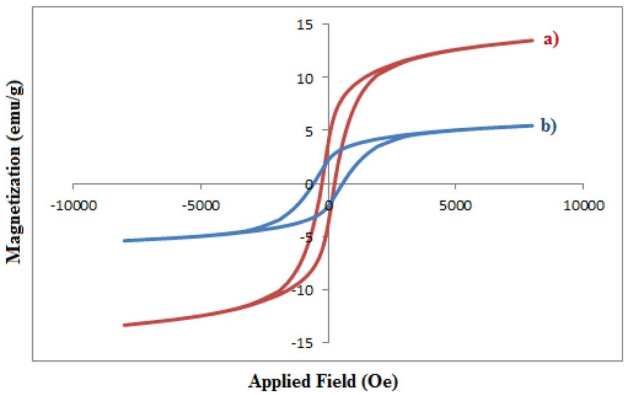

Fig. 7 Magnetization curves of (a) $CuFe_2O_4$ and (b) $CuFe_2O_4$@SiO_2@PTMS@Tu@Ni(II) MNPs

TGA and DSC analysis

Thermogravimetric (TGA) and differential scanning calorimetric (DSC) of $CuFe_2O_4$@SiO_2@PTMS@Tu@Ni(II) MNPs were illustrated in Fig. 8. The figure shows that via the process of dehydration at the programmable heating (30–800 °C) as well as removing of organic moiety, fragmentation and calcination, mass losing of the nanocomposite system was carried out. Observation of the results represented that through the raising of temperature (10 °C/min), overall mass losing of $CuFe_2O_4$@SiO_2@PTMS@Tu@Ni(II) MNPs is 16.17%. In addition, the DSC graph of Ni(II)–$CuFe_2O_4$ system shows that the main mass losing of the nanocatalyst was carried out at 323 °C. These data clearly show that the prepared $CuFe_2O_4$@SiO_2@PTMS@Tu@Ni(II) MNPs has high thermal stability.

Synthesis of biscoumarin materials catalyzed by $CuFe_2O_4$@SiO_2@PTMS@Tu@Ni(II) MNPs

After the successful synthesis and characterization of $CuFe_2O_4$@SiO_2@PTMS@Tu@Ni(II) MNPs, catalytic activity of the prepared nanocatalyst was further studied toward one-pot the Knoevenagel–Michael reaction of 4-hydroxycoumarin with aromatic aldehydes. To optimize reaction conditions, therefore, the condensation reaction of 4-hydroxycoumarin with benzaldehyde was selected as the model reaction and the influence of parameters including the change of reaction-solvent and temperature, using solvent-free conditions and varying the amount of nanocatalyst were studied therein (Table 1). Investigation of the results exhibited that among the examined conditions, using benzaldehyde (1 mmol), 4-hydroxycoumarin (2 mmol) and the Ni(II)–$CuFe_2O_4$ MNPs (10 mg) under solvent-free conditions (70 °C) were the requirements to carry out the titled transformation within 15 min and in high yield. Therefore, the conditions mentioned in entry 13 (Table 1) were selected as the optimum parameters. It is also notable that performing of the model reaction in the presence of $CuFe_2O_4$ MNPs (20–40 mg) did not show any better results under reflux and solvent-free conditions within 120 min (Table 1, entries 1 to 4).

Next, the catalytic activity and usefulness of $CuFe_2O_4$@SiO_2@PTMS@Tu@Ni(II) MNPs were further studied toward one-pot the Knoevenagel–Michael reaction of

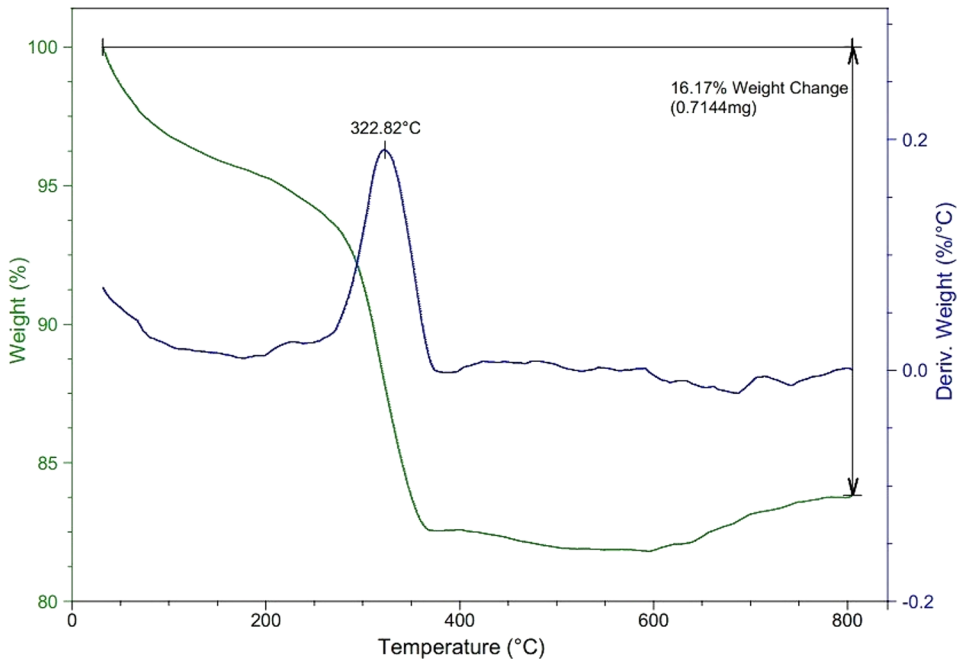

Fig. 8 TGA and DSC analyses of $CuFe_2O_4$@SiO_2@PTMS@Tu@Ni(II) MNPs

Table 1 Optimization experiments for synthesis of 3,3′-(phenylmethylene)-bis(4-hydroxy-2H-chromen-2-one) via the condensation reaction of 4-hydroxycoumarin (2 mmol) with benzaldehyde (1 mmol)

Entry	Catalyst	Catalyst (mg)	Solvent (mL)	Temperature (°C)	Time (min)	Conversion (%)
1	$CuFe_2O_4$	40	Solvent-free	70	120	80
2	$CuFe_2O_4$	20	Solvent-free	70	120	80
3	$CuFe_2O_4$	20	H_2O	Reflux	120	0
4	$CuFe_2O_4$	20	EtOH	Reflux	120	50
5	$CuFe_2O_4$@SiO_2@PTMS@Tu@Ni(II)	70	H_2O	Reflux	120	90
6	$CuFe_2O_4$@SiO_2@PTMS@Tu@Ni(II)	70	EtOH	Reflux	120	70
7	$CuFe_2O_4$@SiO_2@PTMS@Tu@Ni(II)	70	MeOH	Reflux	120	50
8	$CuFe_2O_4$@SiO_2@PTMS@Tu@Ni(II)	70	CH_2Cl_2	Reflux	120	10
9	$CuFe_2O_4$@SiO_2@PTMS@Tu@Ni(II)	70	*n*-Hexane	Reflux	120	0
10	$CuFe_2O_4$@SiO_2@PTMS@Tu@Ni(II)	70	CH_3CN	Reflux	120	0
11	$CuFe_2O_4$@SiO_2@PTMS@Tu@Ni(II)	70	EtOAc	Reflux	120	50
12	$CuFe_2O_4$@SiO_2@PTMS@Tu@Ni(II)	20	Solvent-free	70	15	100
13	$CuFe_2O_4$@SiO_2@PTMS@Tu@Ni(II)	10	Solvent-free	70	15	100
14	$CuFe_2O_4$@SiO_2@PTMS@Tu@Ni(II)	10	Solvent-free	r.t.	60	40

4-hydroxycoumarin with structurally different aromatic, heterocyclic and aliphatic aldehydes at the optimized reaction conditions (Table 2).

Investigation of the results represents that aromatic aldehydes including electron releasing and withdrawing functionalities were easily participated in the condensation reaction using the Ni(II)–$CuFe_2O_4$ MNPs (10 mg) to afford biscoumarin materials within 15–30 min and in high yields. In this context, heterocyclic aldehydes such as furfural and thiophene-1-carbaldehyde as the same of aromatic aldehydes were also successfully performed the titled reaction within 25 min and in 92–95% yields. Consequently, all attempts to examine the reaction of 4-hydroxycoumarin with formaldehyde as an aliphatic aldehyde were also unsuccessful.

In continuation, the suitability of this synthetic method was highlighted by comparison of the obtained result for synthesis of

Table 2 Synthesis of biscoumarin materials catalyzed by $CuFe_2O_4@SiO_2@PTMS@Tu@Ni(II)$ MNPs

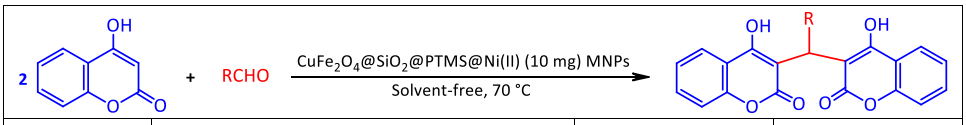

Entry	RCHO	Time (min)	Yield (%)
1	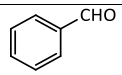	15	95
2	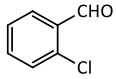	20	92
3	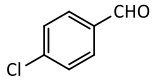	20	92
4	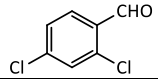	25	93
5	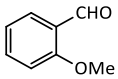	20	92
6	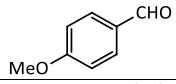	20	93
7	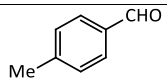	30	93
8	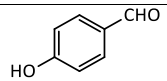	20	94
9	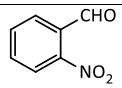	15	96
10	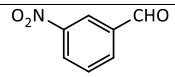	15	95
11	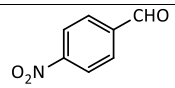	15	96
12	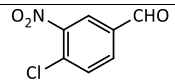	25	95
13	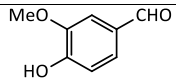	25	93
14	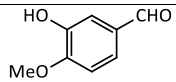	30	93
15	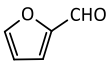	25	92
16	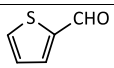	25	95
17		60	0

All reactions were carried out with the molar ratio of aldehyde (1 mmol), 4-hydroxycoumarin (2 mmol) and the Ni(II)–$CuFe_2O_4$ MNPs (10 mg) under solvent-free conditions (70 °C)

3,3′-(phenylmethylene)-bis(4-hydroxy-2H-chromen-2-one) catalyzed by $CuFe_2O_4@SiO_2@PTMS@Tu@Ni(II)$ MNPs with those of reported for other protocols. Table 3 shows that in terms of the yield, reaction time and reusability of the nanocatalyst as well as benefits of solvent-free condition, the present work represents the outstanding result than the previous systems.

Table 3 Comparison of the synthesis of 3,3′-(phenylmethylene)-bis(4-hydroxy-2H-chromen-2-one) with $CuFe_2O_4$@SiO_2@PTMS@Tu@Ni(II) MNPs and other reported systems

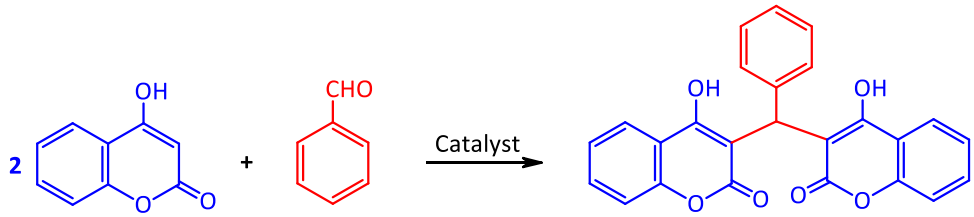

Entry	Catalyst	Time (min)	Yield (%)	Condition	Reusability	Ref.
1	$CuFe_2O_4$@SiO_2@PTMS@Tu@Ni(II)	15	95	H_2O/70 °C	6	Present work
2	I_2	27	93	H_2O/100 °C	–	[60]
3	*n*-Bu_4NBr	30	95	H_2O/100 °C	–	[61]
4	Sulfated titania	15	96	H_2O/80 °C	5	[63]
5	Phosphotungstic acid	20	93	H_2O/80 °C	5	[64]
6	Silica gel	60	95	H_2O/reflux	8	[65]
7	Silica sulfuric acid NPs	20	92	H_2O/reflux	–	[66]
8	$NaHSO_4/SiO_2$	30	90	Toluene/100 °C	3	[69]
9	*p*-Toluenesulfonc acid	70	82	H_2O/reflux	–	[70]
10	RHA-SO_3H	25	92	Solvent-free/80 °C	–	[71]
11	Sodium dodecyl sulfate	150	93	H_2O/60 °C	5	[72]
12	*n*-Dodecylbenzene sulfonic acid	60	87	H_2O/40 °C	–	[73]
13	Graphene oxide nanosheets	15	80	H_2O/reflux	4	[76]
14	Acid-activated montmorillonite	25	95	H_2O/r.t.	6	[77]
15	nano Fe_3O_4@ZrO_2–H_3PO_4	12	97	H_2O/reflux	4	[78]
16	[PSebim][OTf] as IL (ionic liquid)	120	96	IL/70 °C	2	[81]

Although the exact mechanism of this synthetic method is not clear, a depicted mechanism in Fig. 9 shows the promotion role of $CuFe_2O_4$@SiO_2@PTMS@Tu@Ni(II) MNPs in one-pot the Knoevenagel–Michael reaction of aromatic/heterocyclic aldehydes with 4-hydroxycoumarin. The figure shows that via activation of the aldehyde by the Ni(II)–$CuFe_2O_4$ MNPs, nucleophilic attack of 4-hydroxycoumarin with the aldehyde affords 3-(benzylidene)chroman-2,4-dione (**I**). Consequently, the Michael reaction of 4-hydroxycoumarin (second molecule) with the prepared intermediate (**I**) produces the final biscoumarin material.

Recycling of $CuFe_2O_4$@SiO_2@PTMS@Tu@Ni(II) MNPs

The green aspect of the Knoevenagel–Michael reaction of benzaldehyde with 4-hydroxycoumarin in the presence of $CuFe_2O_4$@SiO_2@PTMS@Tu@Ni(II) MNPs was further investigated by examining the reusability of the nanocomposite at the optimized reaction conditions. In this area, once the condensation reaction was completed, the Ni(II)–$CuFe_2O_4$ MNPs were magnetically separated from the reaction mixture, washed with EtOH and then dried under air atmosphere. The vessel of reaction was again charged with the fresh benzaldehyde, 4-hydroxycoumarin and the recycled Ni(II)–$CuFe_2O_4$ MNPs to run the condensation reaction for a second time. Figure 10 represents that $CuFe_2O_4$@SiO_2@PTMS@Tu@Ni(II) MNPs can be reused for six consecutive cycles without the significant loss of catalytic activity. Moreover, VSM (Fig. 11), FT-IR (Fig. 12) and EDX (Fig. 13) spectra of $CuFe_2O_4$@SiO_2@PTMS@Tu@Ni(II) MNPs after first recycling step represent that the magnetic property and structure of the Ni(II)–$CuFe_2O_4$ MNPs remained intact. In this context, the framework stability of the Ni(II)–$CuFe_2O_4$ MNPs was also examined by measuring Ni-content before and after first/second recycling steps of the nanocatalyst. The ICP-OES analysis represents that the percentage of Ni species in the fresh, first and second recycling steps of the nanocatalyst is 19, 18.99 and 18.68%, respectively. Based on these results, it is concluded that the leaching of Ni species in $CuFe_2O_4$@SiO_2@PTMS @Tu@Ni(II) MNPs is negligible.

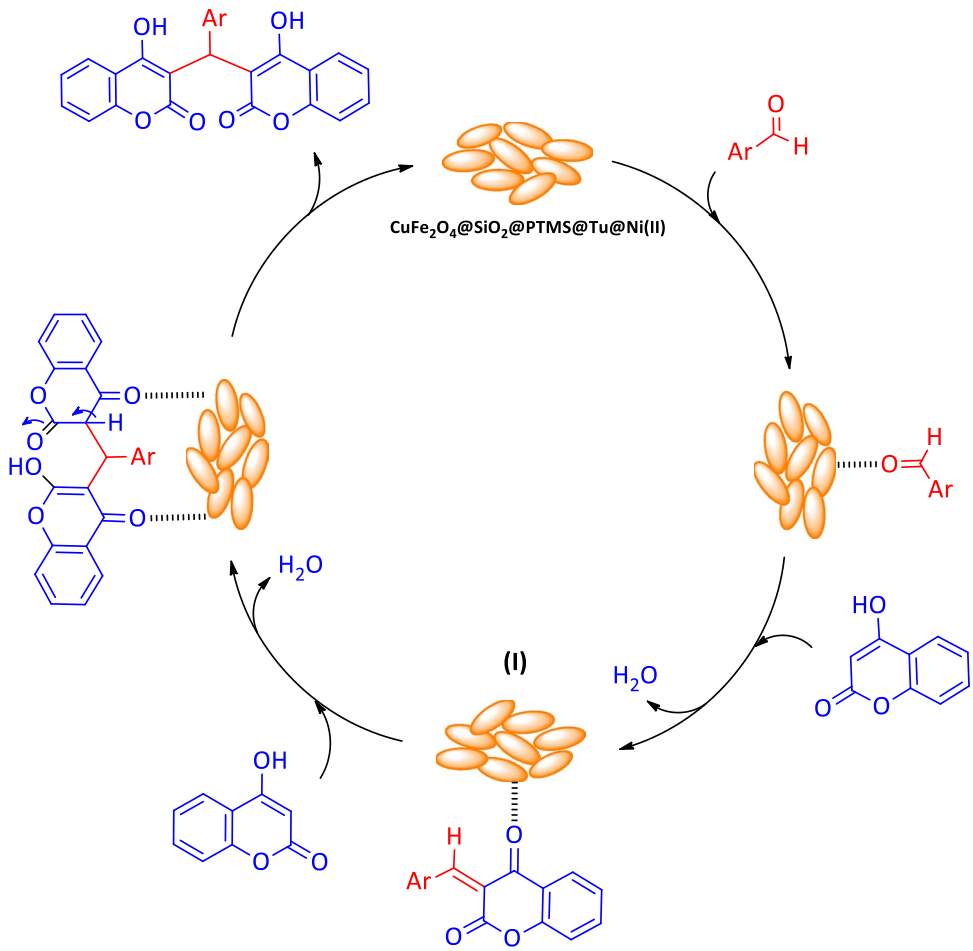

Fig. 9 A proposed mechanism for the promotion role of $CuFe_2O_4$@SiO_2@PTMS@Tu@Ni(II) MNPs

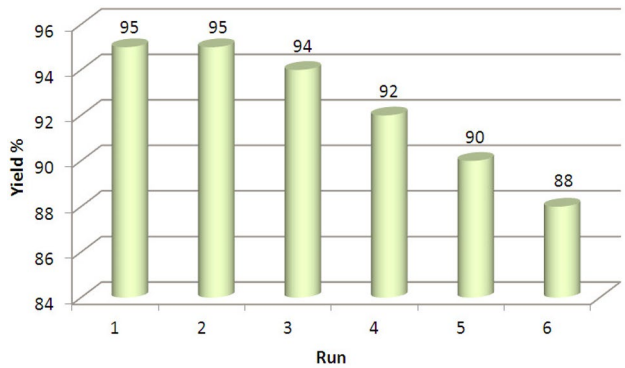

Fig. 10 Reusability of $CuFe_2O_4$@SiO_2@PTMS@Tu@Ni(II) MNPs

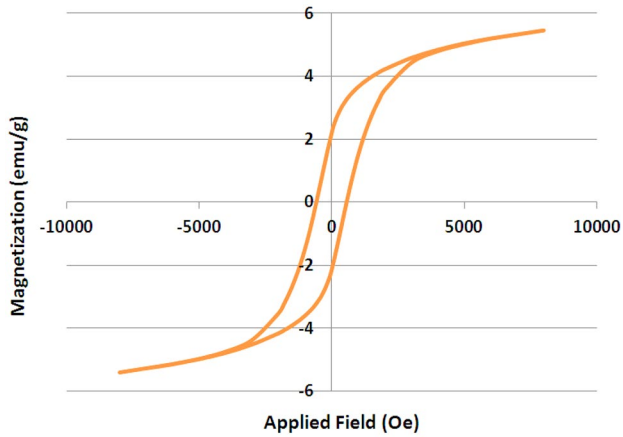

Fig. 11 Magnetization curve of $CuFe_2O_4$@SiO_2@PTMS@Tu@Ni(II) MNPs after first recycling

Conclusion

In this paper, we have synthesized magnetically nanoparticles of the immobilized Ni(II) species on thiourea functionalized copper ferrite: $CuFe_2O_4$@SiO_2@PTMS@Tu@Ni(II). The prepared nanocatalyst system was then characterized using FT-IR, SEM, EDX, XRD, VSM, ICP-OES, TGA and DSC analyses. Catalytic activity of the Ni(II)–$CuFe_2O_4$ MNPs was investigated toward one-pot the Knoevenagel–Michael reaction of 4-hydroxycoumarin with aromatic/heterocyclic aldehydes under solvent-free conditions (70 °C) giving biscoumarin materials within 15–30 min and

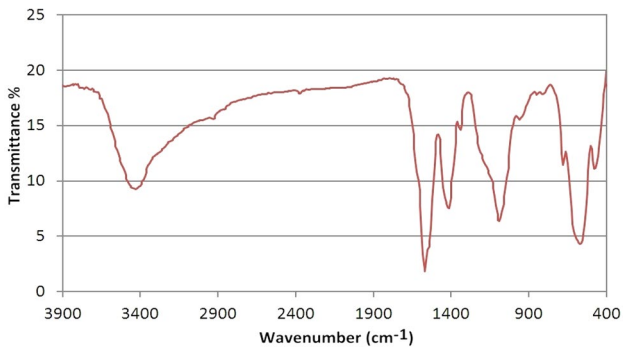

Fig. 12 FT-IR spectrum of $CuFe_2O_4$@SiO_2@PTMS@Tu@Ni(II) MNPs after first recycling

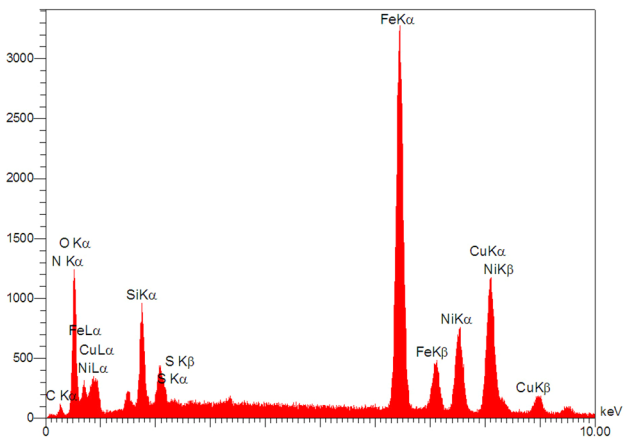

Fig. 13 EDX spectrum of $CuFe_2O_4$@SiO_2@PTMS@Tu@Ni(II) MNPs after first recycling

in high yields. This synthetic method provides the advantages in terms of easy recovering, perfect reusability and low-amount loading of the nanocatalyst, short reaction times and high yield of the products as well as benefits of using solvent-free condition.

Acknowledgment The authors gratefully appreciated the financial support of this work by the research council of Urmia University.

References

1. M.L. Crawley, B.M. Trost, *Applications of Transition Metal Catalysis in Drug Discovery and Development: An Industrial Perspective* (Wiley, New Jersey, 2012)
2. M. Beller, C. Bolm, *Transition Metals for Organic Synthesis: Building Blocks and Fine Chemicals, Second Revised and Enlarged Edition* (Wiley-VCH, Weinheim, 2014)
3. D. Wang, D. Astruc, Chem. Soc. Rev. **46**, 816 (2017)
4. X. Liu, X. Wen, R. Hoffmann, ACS Catal. **8**, 3365 (2018)
5. E.T. Knittl, A.A. Abou-Hussein, W. Linert, Monatsh. Chem. **149**, 431 (2018)
6. A.K. Renfrew, Metallomics **6**, 1324 (2014)
7. K. Hantanasirisakul, Y. Gogotsi, Adv. Mater. **30**, 1804779 (2018)
8. D. Astruc, *Nanoparticles and Catalysis* (Wiley-VCH, Weinheim, 2008)
9. A. Hartwig, *Nanomaterials report,* edited by Deutsche Forschungsgemeinschaft (DFG), ISBN: 978-3-527-33571-8 (Wiley-VCH, Weinheim, 2013)
10. N. Mahata, A. Cunha, J. Orfao, J. Figueiredo, Appl. Catal. A: Gen. **351**, 204 (2008)
11. H. Su, Z. Li, Q. Huo, J. Guan, Q. Kan, RSC Adv. **4**, 9990 (2014)
12. C. Freire, A.R. Silva, Carbon-anchored metal catalysts, in *Carbon Materials for Catalysis*, ed. by P. Serp, J.L. Figueiredo (Wiley, New Jersey, 2009)
13. A.D. Pomogailo, *Catalysis by Polymer-Immobilized Metal Complexes* (CRC Press, Boca Raton, 1999)
14. B.L. Rivas, G.V. Seguel, C. Ancatripai, Polym. Bull. **44**, 445 (2000)
15. F. Sanda, Transition metal containing polymers, in *Encyclopedia of Polymeric Nanomaterials*, ed. by S. Kobayashi, K. Müllen (Springer, Berlin, 2015)
16. P. Nguyen, P. Gómez-Elipe, I. Manners, Chem. Rev. **99**, 1515 (1999)
17. N. Kosinov, C. Liu, E.J.M. Hensen, E.A. Pidko, Chem. Mater. **30**, 3177 (2018)
18. Y. Chai, W. Shang, W. Li, G. Wu, W. Dai, N. Guan, L. Li, Adv. Sci. **6**, 1900299 (2019)
19. Y.X. Tan, F. Wang, J. Zhang, Chem. Soc. Rev. **47**, 2130 (2018)
20. S. Pande, A. Saha, S. Jana, S. Sarkar, M. Basu, M. Pradhan, A.K. Sinha, S. Saha, A. Pal, T. Pal, Org. Lett. **10**, 5179 (2008)
21. S.M. Abdel-Fatah, M. Díaz-Sánchez, D. Díaz-García, S. Prashar, L.H. Abdel-Rahman, S. Gómez-Ruiz, J. Inorg. Organomet. Polym Mater. (2019). https://doi.org/10.1007/s10904-019-01269-y
22. M. Kantam, R. Chakravarti, U. Pal, B. Sreedhar, S. Bhargava, Synfacts **2008**, 0767 (2008)
23. Z. Király, I. Dékány, Á. Mastalir, M. Bartók, J. Catal. **161**, 401 (1996)
24. B. Zeynizadeh, S. Rahmani, RSC Adv. **9**, 8002 (2019)
25. M. Miyagawa, A. Shibusawa, K. Maeda, A. Tashiro, T. Sugai, H. Tanaka, RSC Adv. **7**, 41896 (2017)
26. N. Kalarikkal, S. Thomas, O. Koshy, *Nanomaterials: physical, chemical, and biological applications*, 1st ed., Chapter 14 (Apple Academic Press, New York, 2018)
27. T. Tatarchuk, M. Bououdina, J.J. Vijaya, L.J. Kennedy, *Spinel ferrite nanoparticles: synthesis, crystal structure, properties, and perspective applications*, In: *NANO 2016: nanophysics, nanomaterials, interface studies, and applications*, *Springer Proceedings in Physics*, vol. 195, ed. by O. Fesenko, L. Yatsenko (Springer, 2017), pp. 305–325
28. R. Singh, G. Thirupathi, Manganese-zinc spinel ferrite nanoparticles and ferrofluids. Intech Open Sci. (2017). https://doi.org/10.5772/66522
29. N. Sanpo, C. Wen, C.C. Berndt, J. Wang, Antibacterial properties of spinel ferrite nanoparticles, in *Microbial Pathogens and Strategies for Combating Them: Science, Technology and Education*, vol. 1, ed. by A. Méndez-Vilas (Formatex Research Center, Badajoz, 2013), pp. 239–250
30. A.C.F.M. Costa, A.M.D. Leite, H.S. Ferreira, R.H.G.A. Kiminami, S. Cava, L. Gama, J. Eur. Ceram. Soc. **28**, 2033 (2008)
31. D.S. Mathew, R.S. Juang, Chem. Eng. J. **129**, 51 (2007)
32. B. Gillot, Eur. Phys. J. Appl. Phys. **4**, 243 (1998)
33. S. Yang, W. Xie, H. Zhou, C. Wu, Y. Yang, J. Niu, W. Yang, J. Xu, Tetrahedron **69**, 3415 (2013)
34. P. Niranjan, J.A. Kumar, M. Sasmita, Chem. Lett. **40**, 956 (2011)
35. D. Kundu, N. Mukherjee, B.C. Ranu, RSC Adv. **3**, 117 (2013)
36. M. Gholinejad, B. Karimi, F. Mansouri, J. Mol. Catal. A: Chem. **386**, 20 (2014)

37. B. Zeynizadeh, F. Mohammad Aminzadeh, H. Mousavi, Green Process. Synth. **8**, 742 (2019)
38. B. Zeynizadeh, F. Mohammad Aminzadeh, H. Mousavi, Res. Chem. Intermed. **45**, 3329 (2019)
39. S.M. Sethna, N.M. Shah, Chem. Rev. **36**, 1 (1945)
40. F. Borges, F. Roleira, N. Milhazes, L. Santana, E. Uriarte, Curr. Med. Chem. **12**, 887 (2005)
41. I. Manolov, C. Maichle-Moessmer, N. Danchev, Eur. J. Med. Chem. **41**, 882 (2006)
42. J.C. Jung, O.S. Park, Molecules **14**, 4790 (2009)
43. F.G. Medina, J.G. Marrero, M. Macias-Alonso, M.C. Gonzalez, I. Cordova-Guerrero, A.G. Teissier Garcia, S. Osegueda-Roblesa, Nat. Prod. Rep. **32**, 1472 (2015)
44. A. Stefanachi, F. Leonetti, L. Pisani, M. Catto, A. Carotti, Molecules **23**, 250 (2018)
45. J. Li, X.Y. Xue, X. Li, Z. Hou, X.H. Yang, D. Qu, Y. Zhou, Z.D. Zhang, X.X. Luo, J.T. Li, Arch. Pharm. Res. **39**, 1349 (2016)
46. N. Hamdi, M.C. Puerta, P. Valerga, Eur. J. Med. Chem. **43**, 2541 (2008)
47. Z.H. Chohan, A.U. Shaikh, A. Rauf, C.T. Supuran, J. Enzyme Inhib. Med. Chem. **21**, 741 (2006)
48. I.J. Elenkov, B. Hrvacic, S. Markovic, M. Mesic, A.C. Klonkay, L. Lerman, A.F. Sucic, I. Vujasinovic, B. Bosnjak, K. Brajsa, D. Ziher, N.K. Hulita, I. Malnar, Croat. Chem. Acta **86**, 253 (2013)
49. I. Manolov, C. Maichle-Moessmer, I. Nicolova, N. Danchev, Arch. Pharm. **339**, 319 (2006)
50. J.C. Jung, J.H. Lee, S. Oh, J.G. Lee, O.S. Park, Bioorg. Med. Chem. Lett. **14**, 5527 (2004)
51. C.X. Su, J.F. Mouscadet, C.C. Chiang, H.J. Tsai, L.Y. Hsu, Chem. Pharm. Bull. **54**, 682 (2006)
52. D. Yu, M. Suzuki, L. Xie, S.L. Morris-Natschke, K.H. Lee, Med. Res. Rev. **23**, 322 (2003)
53. H. Zhao, N. Neamati, H. Hong, A. Mazumder, S. Wang, S. Sunder, G.W.A. Milne, Y. Pommier, T.R. Burke, J. Med. Chem. **40**, 242 (1997)
54. M. Choudhary, N. Fatima, K.M. Khan, S. Jalil, S. Iqbal, A.U. Rahman, Bioorg. Med. Chem. **14**, 8066 (2006)
55. I. Kostova, G. Momekov, M. Zaharieva, M. Karaivanova, Eur. J. Med. Chem. **40**, 542 (2005)
56. K.M. Khan, S. Iqbal, M.A. Lodhi, G.M. Maharvi, Z. Ullah, M.I. Choudhary, A.U. Rahman, S. Perveen, Bioorg. Med. Chem. **12**, 1963 (2004)
57. V.D. Kancheva, V.P. Boranova, J. Nechev, I.I. Manolov, Biochimie **92**, 1138 (2010)
58. V. Vahabi, F. Hatamjafari, Oriental J. Chem. **30**, 853 (2014)
59. Z.N. Siddiqui, F. Farooq, Catal. Sci. Technol. **1**, 810 (2011)
60. M. Kidwai, V. Bansal, P. Mothsra, S. Saxena, R.K. Somvanshi, S. Dey, T.P. Singh, J. Mol. Catal. A: Chem. **268**, 76 (2007)
61. J.M. Khurana, S. Kumar, Tetrahedron Lett. **50**, 4125 (2009)
62. F. Shirini, A. Fallah-Shojaei, L. Samavi, M. Abedini, RSC Adv. **6**, 48469 (2016)
63. B. Karmakar, A. Nayak, J. Banerji, Tetrahedron Lett. **53**, 4343 (2012)
64. P. Singh, P. Kumar, A. Katyal, R. Kalra, S.K. Dass, S. Prakash, R. Chandra, Catal. Lett. **134**, 303 (2010)
65. S. Khodabakhshi, M. Baghernejad, Iran. J. Catal. **3**, 67 (2013)
66. B. Sadeghi, T. Ziya, J. Chem. **2013**, 179013 (2013)
67. M.M. Heravi, F. Nahavandi, S. Sadjadi, H.A. Oskooie, F.F. Bamoharram, Synth. Commun. **40**, 498 (2010)
68. K. Niknam, A. Jamali, Chin. J. Catal. **33**, 1840 (2012)
69. V. Padalkar, K. Phatangare, S. Takale, R. Pisal, A. Chaskar, J. Saudi Chem. Soc. **19**, 42 (2015)
70. S. Khodabakhshi, B. Karami, K. Eskandarib, A. Rashidi, South Afr. J. Chem. **68**, 53 (2015)
71. M. Seddighi, F. Shirini, M. Mamaghani, RSC Adv. **3**, 24046 (2013)
72. H. Mehrabi, H. Abusaidi, J. Iran. Chem. Soc. **7**, 890 (2010)
73. B. Pawar, V. Shinde, A. Chaskar, Green Sustain. Chem. **3**, 56 (2013)
74. R. Rezaei, F. Moezzi, M.M. Doroodmand, Chin. Chem. Lett. **25**, 183 (2014)
75. Z. Karimi-Jaberi, B. Masoudi, A. Rahmani, K. Alborzi, Polycycl. Aromat. Compd. **40**, 99 (2020)
76. S. Khodabakhshi, B. Karami, K. Eskandari, S.J. Hoseini, A. Rashidi, RSC Adv. **4**, 17891 (2014)
77. B. Zeynizadeh, S. Rahmani, S. Ilkhanizadeh, Polyhedron **168**, 48 (2019)
78. A. Nakhaei, S. Ramezani, Heterocycl. Lett. **7**, 1035 (2017)
79. K. Kandasamy, M.P. Pachamuthu, M. Muthusamy, S. Ganesabaskaran, A. Ramanathan, RSC Adv. **3**, 25367 (2013)
80. A. Tzani, A. Douka, A. Papadopoulos, E.A. Pavlatou, E. Voutsas, A. Detsi, A.C.S. Sustain, Chem. Eng. **1**, 1180 (2013)
81. W. Li, Y. Wang, Z. Wang, L. Dai, Y. Wang, Catal. Lett. **141**, 1651 (2011)
82. A. Zhu, M. Wang, L. Li, J. Wang, RSC Adv. **5**, 73974 (2015)
83. N. Tavakoli-Hoseini, M.M. Heravi, F.F. Bamoharram, A. Davoodnia, M. Ghassemzadeh, J. Mol. Liq. **163**, 122 (2011)
84. B. Zeynizadeh, I. Mohammadzadeh, Z. Shokri, S.A. Hosseini, J. Colloid Interface Sci. **500**, 285 (2017)
85. Z. Shokri, B. Zeynizadeh, S.A. Hosseini, B. Azizi, J. Iran. Chem. Soc. **14**, 101 (2017)
86. B. Zeynizadeh, Z. Shokri, M.H. Galehban, Appl. Organometal. Chem. **33**, e4771 (2019)
87. S. Karami, B. Zeynizadeh, Z. Shokri, Cellulose **25**, 3295 (2018)
88. S. Karami, B. Zeynizadeh, Carbohyd. Polym. **211**, 298 (2019)
89. M. Gilanizadeh, B. Zeynizadeh, J. Iran. Chem. Soc. **15**, 2821 (2018)
90. B. Zeynizadeh, F. Faraji, RSC Adv. **9**, 13112 (2019)
91. B. Zeynizadeh, S. Rahmani, RSC Adv. **9**, 28038 (2019)
92. B. Zeynizadeh, S. Rahmani, A. Hallaj, Curr. Org. Synth. **16**, 939 (2019)
93. B. Zeynizadeh, M. Sadeghbari, N. Noroozi Pesyan, J. Iran. Chem. Soc. **17**, 73 (2020)
94. B. Zeynizadeh, F. Sepehraddin, H. Mousavi, Ind. Eng. Chem. Res. **58**, 16379 (2019)
95. M. Gholinejad, A. Aminianfar, J. Mol. Catal. A: Chem. **397**, 106 (2015)
96. M. Ragamathunnisa, V.R.E. Jasmine, R. Padmavathy, N. Radha, IOSR J. Appl. Phys. **4**, 5 (2013)
97. Z. Sun, L. Liu, D.Z. Jia, W. Pan, Sens. Actuators, B **125**, 144 (2007)
98. K.R. Reddy, W. Park, B.C. Sin, J. Noh, Y. Lee, J. Colloid Interface Sci. **335**, 34 (2009)